ACS APPLIED MATERIALS & INTERFACES

www.acsami.org

Research Article

Textile Electronics with Laser-Induced Graphene/Polymer Hybrid Fibers

Anna Lipovka, Maxim Fatkullin, Sergey Shchadenko, Ilia Petrov, Anna Chernova, Evgenii Plotnikov, Vitaliy Menzelintsev, Shuang Li, Li Qiu, Chong Cheng,* Raul D. Rodriguez,* and Evgeniya Sheremet

Cite This: https://doi.org/10.1021/acsami.3c06968

Read Online

ACCESS | Metrics & More | Article Recommendations | Supporting Information

ABSTRACT: The concept of wearables is rapidly evolving from flexible polymer-based devices to textile electronics. The reason for this shift is the ability of textiles to ensure close contact with the skin, resulting in comfortable, lightweight, and compact "always with you" sensors. We are contributing to this polymer-textile transition by introducing a novel and simple way of laser intermixing of graphene with synthetic fabrics to create wearable sensing platforms. Our hybrid materials exhibit high electrical conductivity (87.6 ± 36.2 Ω/sq) due to the laser reduction of graphene oxide and simultaneous laser-induced graphene formation on the surface of textiles. Furthermore, the composite created between graphene and nylon ensures the durability of our materials against sonication and washing with detergents. Both of these factors are essential for real-life applications, but what is especially useful is that our free-form composites could be used as-fabricated without encapsulation, which is typically required for conventional laser-scribed materials. We demonstrate the exceptional versatility of our new hybrid textiles by successfully recording muscle activity, heartbeat, and voice. We also show a gesture sensor and an electrothermal heater embedded within a single commercial glove. Additionally, the use of these textiles could be extended to personal protection equipment and smart clothes. We achieve this by implementing self-sterilization with light and laser-induced functionalization with silver nanoparticles, which results in multifunctional antibacterial textiles. Moreover, incorporating silver into such fabrics enables their use as surface-enhanced Raman spectroscopy sensors, allowing for the direct analysis of drugs and sweat components on the clothing itself. Our research offers valuable insights into simple and scalable processes of textile-based electronics, opening up new possibilities for paradigms like the Internet of Medical Things.

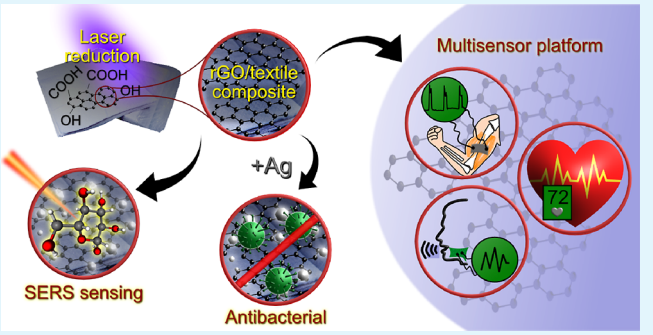

KEYWORDS: *laser processing, textile sensor, graphene composite, conductive textile, wearables*

INTRODUCTION

Improving the quality of life is closely tied to advancements in comfort and health. It forces modern devices, including wearables, to fulfill new functionality and performance requirements.[1] In this context, an attractive concept is the development of sensors integrated into everyday clothes to ensure direct contact with the skin, reliable sensing, and continuous monitoring of health indicators.[2] Introducing electrical conductivity to the textiles upgrades the conventional fabrics to the level of wearable sensor platforms.[3] Up to date, one of the most efficient ways to achieve this is the metallization of textiles that exhibits the values of sheet resistance down to 0.02 Ω/sq, while maintaining the original knitted fiber structure.[4] However, this strategy could hardly be considered cost-efficient. An alternative is using carbon nanomaterials such as nanotubes or graphene,[5] which significantly increase surface area and electrical conductivity critical for textronics, while being less expensive.

In addition to high conductivity, which could also be achieved with conductive inks,[6,7] the challenge is to develop the technology that allows to preserve electrical, mechanical, and structural properties for extended periods of wearing. Moreover, the approach must be adjustable, scalable, and easy to perform to become widely adopted. Laser processing is excellent for addressing these challenges, offering additional benefits such as free-form patterning and eco-friendliness compared to chemical and thermal methods.[8] Previously, we showed that laser processing produces a resilient graphene/polymer nanocomposite with polyethylene terephthalate sheets.[9,10] In this work, we devised a strategy to integrate

Received: May 17, 2023
Accepted: July 10, 2023

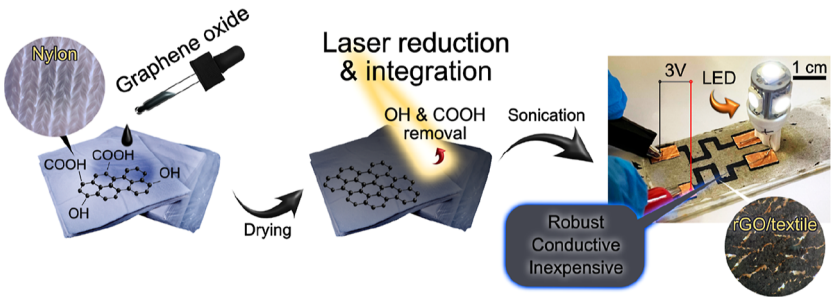

Figure 1. Schematic illustration of the rGO/textile composite fabrication steps and demonstration of an actual circuit used to light an LED.

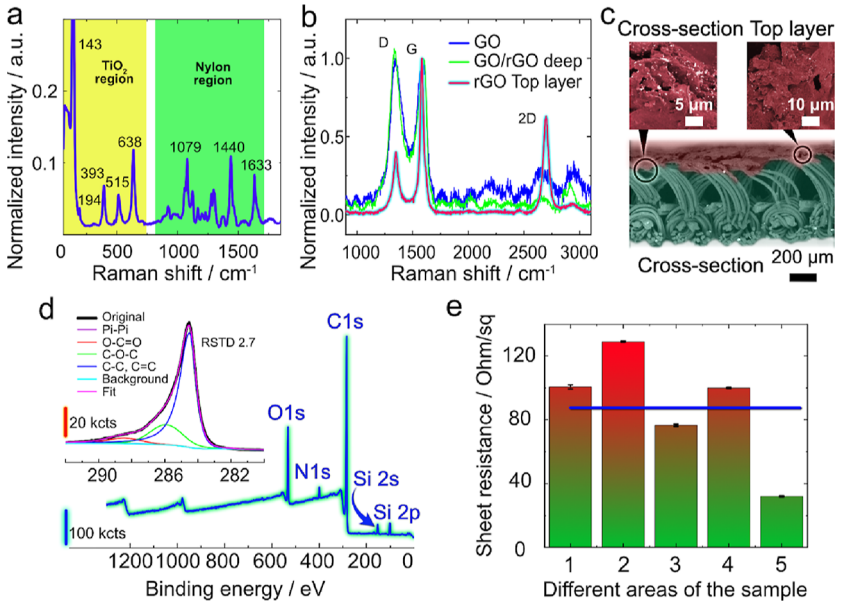

Figure 2. Characterization of rGO/nylon textile composites. (a) Raman spectrum of nylon textile; (b) Raman spectrum of nylon covered with a thick GO film, and two spectra after laser reduction recorded on the surface and on the underlying fibers; (c) SEM images of the top surface and cross-section; (d) XPS survey spectrum and narrow C 1s region; (e) sheet resistance of the composite with the average value of 87.6 ± 36.2 Ω/sq. The values obtained in different spots of the same rGO/textile sample.

graphene into nylon-based textiles in an elegant and efficient manner. These graphene/textile composites are sensitive to deformation and could serve the development of a wide range of sensors.

Wearable sensors that utilize hydrophilic fabrics may create a suitable environment for bacterial growth when combined with dirt and sweat.[11] Therefore, it is crucial to ensure that wearable sensors are effective and safe from biohazards. While most bacteria are harmless, some pathogenic microorganisms, such as *Trichophyton interdigitale*, *Streptococcus viridans*, *Streptococcus nonhemolyticus*, or *Blastomyces*, could cause serious infectious diseases. One way to tackle this issue is by incorporating antibacterial properties into textile sensors.[12] To this end, the most efficient approach is functionalizing the fabric with metals, metal oxides, and metal nanoforms (Ag, Cu, Au, and Zn NPs).[13] Silver is the most promising among these due to its complex interaction mechanism with cells. The synthesis of silver nanoparticles is straightforward and typically executed following well-established chemical or electrochemical routes.[14] We found that in addition to the original laser-assisted graphene oxide (GO) photoreduction and composite formation, lasing enables the integration of silver *via* the photochemical reduction of silver ions from $AgNO_3$ to form Ag clusters and make the textiles safer to use.[15]

Utilizing inexpensive materials, scalable laser processing technology, and incorporating antibacterial properties enables a safe multisensor platform on textiles with excellent performance to contribute to key technologies such as wearables and smart clothes.

RESULTS AND DISCUSSION

Laser-Driven Processes Behind rGO/Textile Composite. To face the challenge of modern textronics, we designed a two-step strategy to functionalize synthetic textiles with high-quality reduced graphene oxide (rGO), as schematically shown in Figure 1. First, white nylon textile was coated with a 4 mg/mL GO water dispersion. We observed a uniform textile surface coverage (see Figure S1) thanks to GO hydrophilicity that helped to form multilayers on fibers due to strong van der Waals and H-bonding interactions.[16] Then, once dried, the GO textile was laser processed to reduce GO and make the fabric electrically conductive. The laser-induced removal of oxygen-containing groups from GO has been known since pioneering work in 2009.[17] However, the optical properties of the film, choice of the substrate, and tuning of processing parameters make a significant difference in light-matter interactions and properties of the resulting laser-processed material. We found that laser irradiation did not only reduce

https://doi.org/10.1021/acsami.3c06968
ACS Appl. Mater. Interfaces XXXX, XXX, XXX−XXX

GO, but simultaneously integrated freshly formed rGO to the textile surface. This finding is critical because we intermixed graphene with the polymer matrix and increased the textile's active surface area besides the electrical conductivity. Excited by this result, we anticipated that such textile functionalization could be kept for an extended period. This expectation was encouraged by the ultrasonication process of the hybrid textiles to remove the remaining GO and burnt byproducts that were loosely attached. This simple experimental implementation led us to graphene/textile platforms that we further investigated as robust multifunctional sensors.

Originally, we were planning to form single-step laser-induced graphene (LIG) directly on textiles without the use of any additional nanomaterials. However, even a relatively gentle laser treatment in the visible range did not prevent partial fiber destruction, which was a universal effect for the 15 different textile types we irradiated (Note S1). The irreversible damage of fibers would significantly limit the use of LIG alone in real applications. To avoid this undesirable effect and preserve the textile properties, we introduced a GO film as an additional carbon precursor and performed its further laser processing on the surface of the textile as discussed above. The irradiation of this system resulted in a less disrupted electrically conductive textile surface.

Laser reduction of GO reverts most of the carbon atoms from the sp^3 to sp^2 hybridization state, partially recovering the graphene structure. We estimated the quality of reduction with Raman spectroscopy, an especially useful tool for carbon nanomaterial characterization.[18] The original textile revealed five characteristic peaks at 143, 194, 393, 515, and 638 cm^{-1} (Figure 2a) assigned to E_g, E_g, B_{1g}, B_{1g}, and E_g modes of the anatase phase of TiO_2, which is conventionally used as a white dye for textiles.[19] The lower energy region contained active modes of nylon fibers themselves, with sharp peaks at 1079, 1440, and 1633 cm^{-1} assigned to C−C stretching, CH_2 bending, and amide I vibrations, respectively.[20] The thick GO film screens the signal from the textile, as evidenced by the dominance of defect-activated D and sp^2 carbon G Raman bands from GO (Figure 2b). The changes induced by the laser should mainly occur on the utmost fibers of the textile. We investigated the surface layer and the underlying fibers, which are easily distinguishable with an optical microscope. On the top layer (Figure 2b), we observed a decrease in the D/G intensity ratio from 1.0 to 0.4 due to GO reduction. At the same time, the second-order graphene bands appeared with the most intense 2D band - overtone of the D band activated by a double resonance process.[21] In our case, the 2D/G intensity ratio was equal to 0.7, a typical value for multilayer graphene that confirms the relatively high graphitization.[22] This result could be attributed either to efficient GO reduction or LIG formation from the polymer or, most likely, to both processes simultaneously. On the other hand, Raman spectra recorded from the deeper layers have no difference from the spectra of unmodified GO, which means that the underlying GO layers do not undergo reduction or get just slightly reduced with a highly defective structure.[23]

The brown and relatively thick GO film in our system acts as a photothermal transducer, efficiently absorbing light and triggering the polymer phase transition to liquid. The high photon flux leads to the formation of a graphene/textile hybrid only at the top layer, keeping the initial properties of the underlying bulk textile intact. Previously, rGO/polyester and rGO/cotton fabrics were reported for flexible, free-standing, highly conductive, and robust wearable sensors and smart clothes.[5,24] However, those recent reports used chemical and thermal reduction routes, both of which convert the whole GO volume with no spatial selectivity and thus have limitations in tuning the material properties and free-form patterning into specific shapes. So far, the most successful attempt to create an rGO/nylon composite was accomplished by chemical GO reduction with subsequent laser patterning to fabricate textile capacitors.[25] In contrast, we used laser patterning alone to obtain a well-developed intermixed melted nylon/rGO system. This hybrid structure is demonstrated on the scanning electron microscopy (SEM) cross-section images in Figure 2c. The graphene/nylon composite thickness reached 120 μm, with the thickness of unmodified textiles below ca. 650 μm. X-ray photoelectron spectroscopy (XPS) allowed for analyzing more precisely the surface condition after composite formation. The survey spectrum in Figure 2d shows the conventional C 1s and O 1s bands, also indicating a minor presence of N and Si originating from the textile itself. The C/O at. % ratio equals 7.6, compared to 4.9 for the unmodified textile (see survey spectrum in Note S2 and Figure S2). This value increased because of the surface carbonization caused by GO reduction and LIG formation, which is in agreement with Raman spectroscopy results. The C 1s region (Figure 2d) was deconvoluted into four components, with the dominant sp^3 and sp^2-hybridized carbon in the forms of C−C and C═C (284.5 ± 0.1 eV) bonds, which is typical for graphene materials.[26]

The direct and most valuable effect we obtained from GO reduction was the drastic change in electrical properties. The initially insulating textile turned highly conductive, with an average sheet resistance of 87.6 ± 36.2 Ω/sq (5 different sample areas were analyzed, see Figure 2e). This is a remarkable difference, especially considering that these values were obtained after subjecting the sample to ultrasonic bath cleaning for 1 minute before the measurements. We also examined whether the textiles would maintain their electrical performance under extended exposure to ultrasound (Figure S3). Even after 5 minutes of sonication, we found that sheet resistance changes were minimal and within the error bars. The textiles also kept their electrical conductivity after washing with detergents imitating their use in real-life conditions. After five washing cycles, rGO/textiles maintained resistance values within the 2−11 kΩ range, indicating no visual changes or signs of surface degradation (Note S3 and Figures S4, S5). In addition to washing the textiles, we investigated the stability of their performance in phosphate-buffered saline (PBS) and artificial sweat to imitate harsh wearing conditions. The textiles remained conductive in the kΩ range after 18 days in PBS, and after 5 days in artificial sweat (Figure S6). The rGO/textiles also survived ten cycles of stripping with an adhesive tape, maintaining the resistance in the Ω range, while additional cycles shifted the values to the kΩ range (Figure S7).

While this work is focused on fabricating new hybrid textiles and developing wearable sensors, our results are promising for the future research on smart clothing, which should include a more detailed investigation of their mechanical properties and long-term performance. So far, we have examined the stretchability of our textiles by recording a stress−strain curve. Our findings indicate that the materials have an elongation at break of ∼881%, while pristine textiles are less stretchable with a value of ∼604% (Figure S8). Even counting that the original textiles can bear more stress (5.7 MPa at break

https://doi.org/10.1021/acsami.3c06968
ACS Appl. Mater. Interfaces XXXX, XXX, XXX−XXX

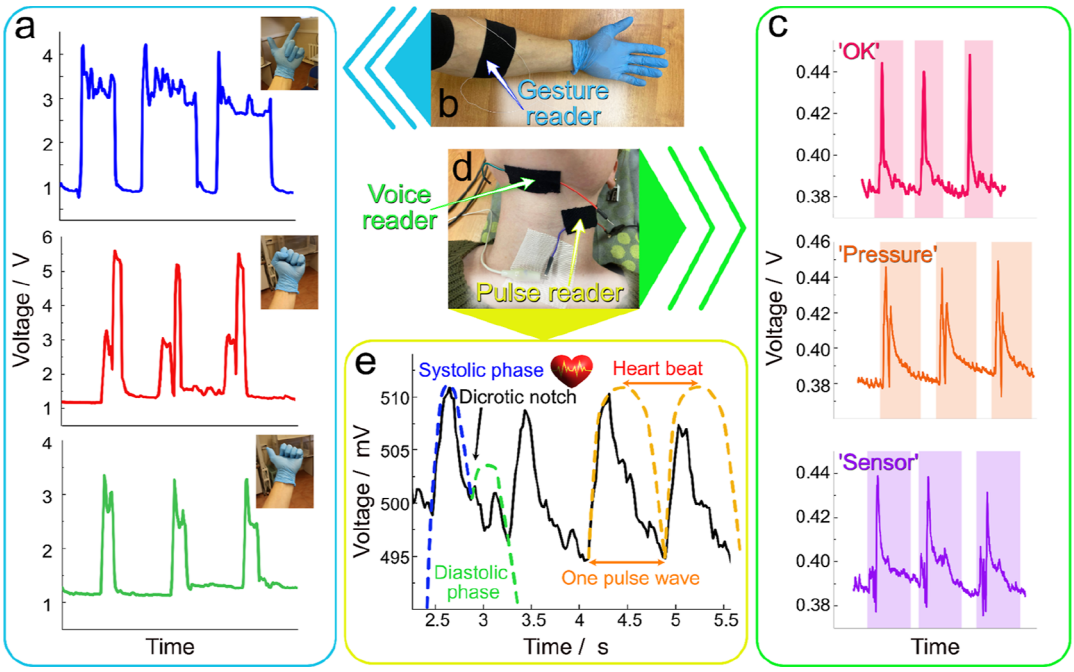

Figure 3. rGO/nylon composites used as wearable sensors. (a) voltage recording of muscle activity sensor performance using several different gestures; (b) the placement of a gesture sensor on the hand; (c) demonstration of the voice recognition sensor; (d) the placement of the voice and pulse sensors on the neck; and (e) pulse recording.

compared to about 0.7 MPa for rGO/textiles), it is not crucial for clothing textiles. What is more critical is the significantly larger linear range of elastic deformation for rGO/textile (>800% strain *vs* <300 for the unmodified fabric). The extended linearity range is a useful improvement for apparel intended for daily wearing. This effect can be attributed to the reinforcement of textiles with rGO flakes and the bonding of fibers due to polymer melting. Indeed, the stress−strain curve for unmodified textiles shows some perturbations caused by the breakage of individual fibers. In contrast, the rGO/textile sample has a smooth linear curve since the material represents a more integral structure with interconnected fibers. Our results demonstrate that these multifunctional textiles can withstand typical mechanical stresses encountered during wear.

Development of Wearable Sensor Platform. Our hybrid structures unlocked the options for several attractive applications, particularly in textile-based sensors, due to their lightweight nature, ability to remain conductive after washing and ultrasonication, and high level of customizability in size and shape. To demonstrate the textiles potential, we first fabricated a gesture recognition sensor to evaluate the sensitivity of our textile composites to muscle deformation. Figure 3a shows the voltage change over time under a constant current for three different gestures, each repeated three times. The sensor deformation caused by muscle activity resulted in distinguishable signal shapes with an immediate response for each repetition. We tested several different gestures (see Note S4 and Figure S9). The signal responses were reproducible, making all six gestures individually recognizable. For these measurements, the sensor was placed on the brachioradialis muscle, as shown in Figure 3b. In this case, the sensing mechanism relies on graphene/textile deformation, which changes the distance between the conductive sites. Consequently, these changes induce variations in electrical resistance and/or interlayer capacitance.

Excited by the excellent performance of rGO/textile for gesture tracking, we explored the detection of more subtle deformations. Following recent demonstrations on graphene foams,[27] we designed voice and heartbeat sensors. Using the voice sensor, we obtained clear, distinguishable, and repetitive signals for the words "Ok", "Pressure", and "Sensor" (Figure 3c). The different signal shapes, caused by the comprehensive muscle movements during the speech, prove that the rGO/textile composite could further serve for voice recognition applications.[28] Same as in the previous case, the resistance perturbations induced changes in voltage under constant current. The resistance variations are attributed to deformations initiated by larynx movement and vocal cord vibrations that generate an increase and decrease between the rGO conductive sites. Besides distinguishing the words, we also recorded signals from prolonged sounds like "R" and guttural "A" (Note S5 and Figure S10). Particularly these sounds induce strong vibrations of the throat and cause instant sensor response with a high signal intensity. Notably, deep guttural sounds result in a signal decrease, while "R" and any word pronunciation increase the signal. This is explained by the physiological differences in pronunciation.

Finally, we recorded the heartbeat signal by placing the sensor over the carotid artery area at the neck, as shown in Figure 3d. This configuration allowed not only to record heart rate, but also to follow pulse wave dynamics. Figure 3e shows repetitive peaks attributed to heart contraction phases. The volunteer's pulse in a relaxed state was 76 beats per minute (healthy values for adults range from 60 to 100 bpm).[29] A sharp rise at the beginning of a wave that lasts about 0.4 s correlates with the ventricle systole. The systolic phase starts at 0.4 s. The dicrotic notch is recorded between the systolic and diastolic phases and is associated with the end of contraction and return of blood flow to the heart. After that, there is another rise associated with the diastolic phase and closed heart valves. Finally, the aorta narrows, and the pressure drops

https://doi.org/10.1021/acsami.3c06968
ACS Appl. Mater. Interfaces XXXX, XXX, XXX−XXX

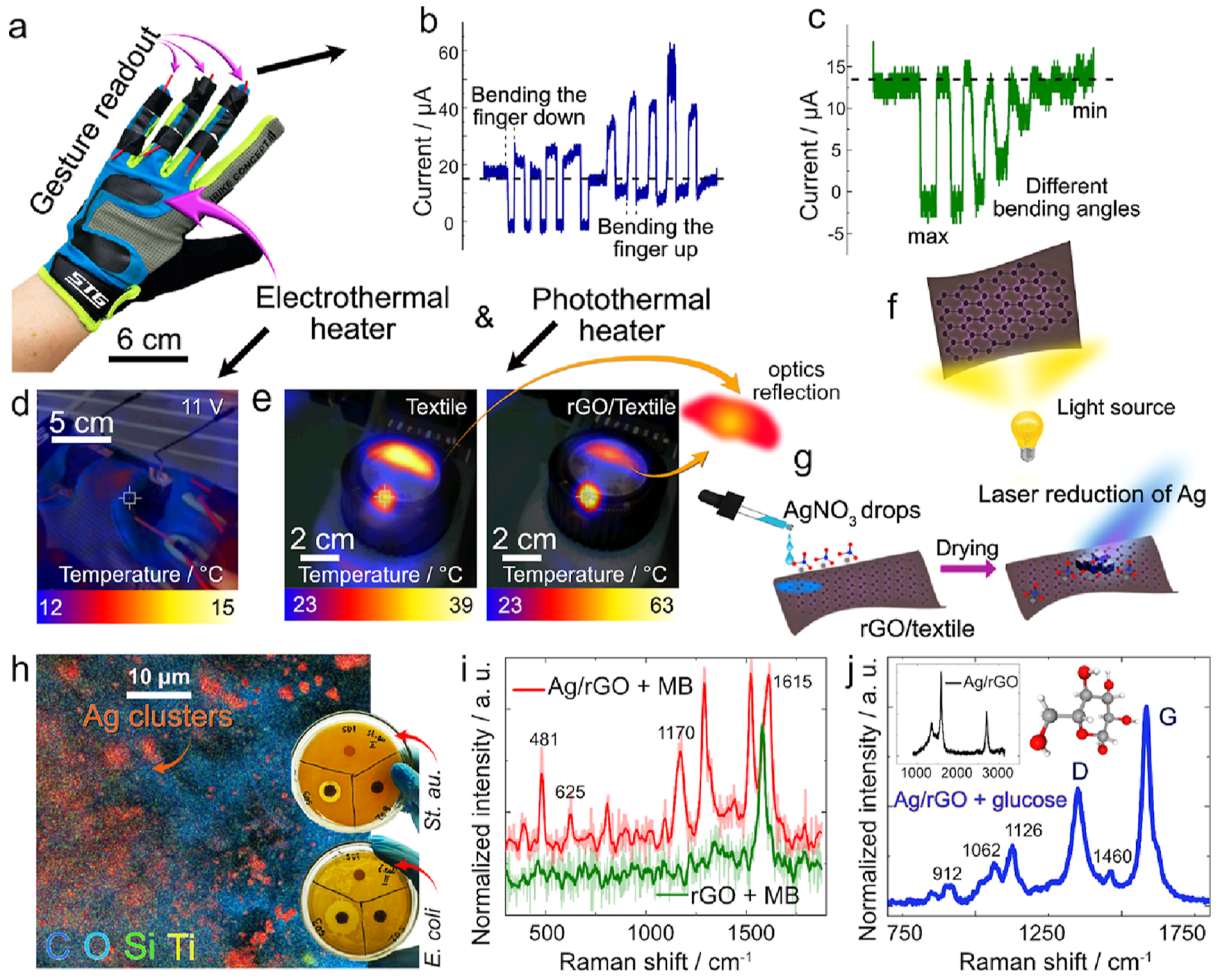

Figure 4. (a) Nylon/spandex/polyester glove with 4 integrated rGO/textile sensors: 3 bending sensors on the middle, ring, and little fingers, and an electrothermal heater on the back side of the hand; (b) current response on bending the finger up and down; (c) current response on changing the bending angle; (d) electroheating of the glove in the fridge; (e) thermal camera images of photoinduced heating of rGO/textile composites; (f) a scheme of the photoheating experiment; (g) a scheme of the textile functionalization with Ag nanoparticles; (h) EDX mapping of the surface of Ag/rGO/textile and inhibition zones of the growth of *E. coli* and *St. aureus* bacteria on a Petri dish after 24 h of cultivation. Orange color represents the distribution of Ag, while blue stands for C, light blue for O, green for Si, and yellow for Ti; (i) SERS detection of MB on Ag/rGO/textile together with a reference sample without silver functionalization; (j) SERS detection of glucose (2.2 M) on the surface of Ag/rGO/textile together with the Raman spectrum recorded from the sample (inset).

until heart returns to the systolic phase. All these changes were successfully recorded by the textile sensor we designed.

The sensitivity to such low-intensity vibrations and deformations made a great foundation to implement our devices in smart clothes and wearable sensors. To go beyond laboratory demonstrations, we adapted a commercially available glove made of nylon (with some fractions of spandex and polyester), and used our method to fabricate graphene composites directly on the glove's surface (Figure 4a). We integrated three bending sensors on the glove's fingers and an electrothermal heater on the back of the hand, which is especially useful in winter and cold climates. Figure 4b shows the sensor response to bending the finger up and down from the neutral position (fingers parallel to the hand palm) with a change of the signal following the fingers' motion and the distance between the conductive sites, respectively. Moreover, the response varies according to different bending angles, and the device is sensitive even to barely noticeable movements of the finger, as shown in Figure 4c. This exciting demonstration opens up new opportunities for our textiles in soft robotics. The electrothermal heater's performance was verified by placing the glove inside a fridge to imitate cold temperatures (Figure 4d). The composite area could be heated up to 48 °C by applying the voltage from 11 to 40 V (see Note S6 and Figure S11). These results could be helpful in thermal therapy, which usually requires temperatures of 40−50 °C.[3,30] Moreover, by decreasing the heater size, we reached temperatures as high as 112 °C under 12 V (Note S6 and Figure S12).

Besides electrical stimulation, we found that our textiles could be heated up with light from a halogen lamp (Figure 4e) or less intensely under an LED (Note S7 and Figure S13). We estimated the temperatures we could reach with a lamp using the setup presented in Figure 4f. Illumination of the clean nylon textile increased its temperature to 39 °C (room temperature was ∼23 °C), while the rGO/textile composite reached 63 °C within a few seconds. This opens promising perspectives toward self-sterilization of clothes and virus inactivation *via* photothermal heating, which the world requires these days. For instance, the spike protein in the COVID-19 virus is sensitive to temperature and becomes inactive after 90 minutes at 56 ± 2 °C, which could be easily reached using our multifunctional textiles.[31]

https://doi.org/10.1021/acsami.3c06968
ACS Appl. Mater. Interfaces XXXX, XXX, XXX−XXX

Table 1. Growth Suppression of Bacteria *E. coli* and *St. aureus* by the Test Samples on the Surface of the Nutrient Medium after 24 h of Cultivation

Sample	Fabrication details	Width of the growth inhibition zone	
		E. coli	*St. aureus*
Textile	No modifications	✗ no inhibition zone	✗ no inhibition zone
rGO/textile	rGO/nylon composite	✗ no inhibition zone	✗ no inhibition zone
Ag/rGO/textile	Laser deposition of AgNPs on the top of rGO/textile surface	✓ (27.9 ± 4.8) mm	✓ (18.1 ± 1.0) mm

rGO/Textile Composites Functionalization with Silver. We made our textiles antibacterial, aiming at increasing their value as healthcare platforms. That was achieved by functionalization of rGO/nylon surfaces with Ag nanoparticles *via* laser-driven photoreduction (Figure 4g). Combining GO reduction with a subsequent Ag NPs integration for smart textiles is a powerful approach under intense development. For instance, it was reported that rGO combined with silver deposited by chemical reduction and thermal annealing increased the durability of polyethylene terephthalate (PET) textiles.[32] The use of the laser to grow silver NPs from $AgNO_3$ was already discussed and implemented by us for graphene surfaces.[15] In our study, we used laser irradiation to photochemically reduce an $AgNO_3$ aqueous solution onto the rGO/textile surface and embed metallic nanoparticles, eliminating the need for additional functionalization techniques or reducing chemicals to create antimicrobial agents. EDX (energy-dispersive X-ray spectroscopy) mapping in Figure 4h shows the successful formation of silver particles and clusters distributed on the top of the rGO/textile surface. To better understand the structure and size of silver clusters and their particle shapes, we conducted further EDX mapping at higher magnification. Additionally, we captured a SEM image of an individual particle, revealing its spherical shape and approximately 300 nm size (see Figures S14 and S15). XPS analysis directly confirmed the functionalization of the textiles with silver and its reduction to a zero-valence state (see Figure S2). Ag 3d narrow region indicates the appearance of two silver bands deconvoluted to four peaks responsible for metallic silver: Ag $3d_{5/2}$ (Ag^0) at 367.8 ± 0.1 eV and Ag $3d_{3/2}$ (Ag^0) at 373.8 ± 0.1 eV; and for ionic silver: Ag $3d_{5/2}$ (Ag^+) at 368.2 ± 0.1 eV and Ag $3d_{3/2}$ (Ag^+) at 374.3 ± 0.1 eV, evidencing partial conversion of Ag^+ to Ag^0. In this case, C 1s narrow region shows a rise of C═C bond compared to silver-free rGO/textile. This means that the second round of laser processing contributed to Ag reduction as well as to simultaneous rGO reduction to a higher degree.

To experimentally verify antibacterial properties, we investigated the initial nylon, rGO/textile, and Ag/rGO/textile samples' responses against *Escherichia coli* and *Staphylococcus aureus* (*St. aureus*). These two strains were selected due to their distinct cell wall structures and representation of two major groups of bacterial infections. *E. coli* is a Gram-negative bacillus found in the gut microbiota of humans. On the other hand, *St. aureus* is a Gram-positive coccus found on the skin and in the upper respiratory tract of humans, which could become pathogenic and cause serious health issues. The textiles' antibacterial performance was evaluated using the disk diffusion test, as shown in Table 1. We expected the nylon sample to have no inhibition zone, but as for rGO—there was no explicit expectation. The antibacterial activity of rGO has been a subject of debate in the literature. Some studies have experimentally demonstrated the antimicrobial effect of rGO, attributing it to oxidative stress and damage caused by the graphene's sharp edges when in contact with bacterial cells.[33,34] However, it has also been highlighted that this effect depends on the concentration of graphene oxide (GO) and the specific synthesis protocol.[35] Even if rGO alone in the form of a dispersion or powder might exhibit antibacterial properties, the mixture of rGO flakes with non-antibacterial nylon is unlikely to be antimicrobial due to the significant contribution of the substrate and partially interrupted graphene network. RGO/textile samples did not show any inhibition zone in our experiments. On the other hand, Ag/rGO/textile showed a considerable inhibition zone for both *E. coli* (27.9 ± 4.8 mm) and *St. aureus* (18.1 ± 1.0 mm), demonstrating a significant antibacterial effect (Figure 4h and Table 1). The larger inhibition zone for Gram-negative bacteria is associated with a thin peptidoglycan layer and an outer lipid membrane, which is the opposite for Gram-positive ones. The antibacterial effect of Ag/rGO/textile is attributed to the presence of both silver ions and silver nanoparticles. The mechanism could be connected to Ag adsorption on negatively charged cell walls, which causes their damage, or to a membrane destabilization, resulting in a cellular content leak. Both processes lead to cell death.[36,37]

Silver functionalization of textiles does not only induce antibacterial activity but also could be useful to create a wearable surface-enhanced Raman spectroscopy (SERS) sensor. Since nylon is widely used in sportswear, Ag/rGO/textile could potentially offer valuable insights for the user, for instance, by analyzing sweat during physical activities. Non-invasive detection of drugs and hormones in sweat is a currently developing field with numerous challenges.[38] First, we used methylene blue (MB) as an analyte to see if our textiles showed the SERS effect. MB is a water-soluble dye typically used for SERS sensing demonstrations. On the surface of Ag/rGO/textile, we observed typical MB Raman peaks at 481, 625, 1170, 1290, 1524, and 1615 cm^{-1} corresponding to δ(C−N−C), δ(C−S−C), β(C−H), υ(C−N), υ_{asym}(C−C), and υ(C−C) ring vibrations, respectively.[39] When we recorded the spectrum on the same textile without silver functionalization, there were no indications of MB, as demonstrated in Figure 4i. Building on the success of MB SERS sensing results, we conducted a proof-of-concept SERS detection of glucose, as shown in Figure 4j. We placed a drop of glucose solution (2.2 M) onto the Ag/rGO/textile surface, and immediately

https://doi.org/10.1021/acsami.3c06968
ACS Appl. Mater. Interfaces XXXX, XXX, XXX−XXX

performed SERS measurements. The glucose bands at 850, 912, 1062, 1126, and 1460 cm^{-1} are assigned to C−C stretching, C−OH stretching, C−O stretching, C−O−H bending, and CH_2 stretching, respectively.[40] However, to be practical for real-world applications, the sensitivity must be enhanced to detect glucose concentrations below 0.2 mM, which is the level found in human sweat.[41] Such application-target optimization is possible thanks to laser processing, which allows tuning the amount and size of Ag NPs clusters, the quality of rGO/textile surface morphology, and other factors contributing to the material application and performance in wearable sensors.

In this work, we got unique insights into fabricating a flexible multifunctional textile platform with laser processing, making a solid and scalable foundation for future advancements in textile electronics.

CONCLUSIONS

Wearable and affordable sensors are no longer a matter of future developments but fundamental and engineering projects. This work makes a step toward efficient and inexpensive textile sensor platforms. We showed for the first time a simple and scalable way to fabricate thin and lightweight rGO/nylon composites by laser processing with a wavelength in the visible range. Simultaneous photonic-driven reduction of GO and integration of rGO to the polymeric textile surface results in highly conductive (tens of Ω/sq) textiles that retain their performance after sonication and washing. Considering the ease of fabrication and surface properties, we found great use of our composites as deformation sensors for gesture recording, real-time pulse measurements, and voice recognition. All sensors showed immediate responses to different stimuli. We also implemented three bending sensors and an electrothermal heater within a single system embedded in a commercial glove made from a nylon/spandex/polyester mixture. To contribute to personal healthcare, we made an additional step and functionalized our textiles with silver clusters using the same laser processing approach. This functionalization resulted in introducing antibacterial properties to our textiles. *In vitro* disk diffusion tests on Ag/rGO/textile composites showed an inhibition zone with Gram-negative (27.9 ± 4.8 mm) and Gram-positive (18.1 ± 1.0 mm) bacteria. Benefiting from additional silver integration, we implemented a proof-of-principle SERS sensor to detect a model dye analyte and glucose. This research paves the way for developing safe and comprehensive multisensor platforms that can be directly integrated into everyday fabrics.

METHODS AND MATERIALS

Materials. The textile composition represents 88% nylon and 12% spandex, according to the specification from the manufacturer. GO water dispersion (4 mg/mL) was purchased from Graphenea. The glove for the sensors contains 70% nylon, 20% polyester, and 10% spandex. The muscle activity, pulse, and voice recognition sensors were fixed using kinesiology tape Rocktape H2O. For SERS sensing, glucose (2.2 M) was purchased in a local pharmacy, and Methylene Blue from Sigma-Aldrich.

Sensor Fabrication. GO was placed on the top of the textile using drop coating, with the amount depending on the sample size to form a thick film, counting 1.5 μL of dispersion per 1 mm^2. The film was dried on the heating plate at 50 °C. The laser processing was performed using a 436 nm pulse laser, with pulse energy—150 mJ, pulse frequency—2.8 kHz, and pulse duration—250 μs. Fabricated samples were rinsed with distilled water and sonicated for 10 min to remove non-integrated nanomaterials. For the disk diffusion test, 40 μL of 0.1 M $AgNO_3$ aqueous solution was applied to the surface of rGO/textile and laser processed while wet. The samples were dried and cut into 10 mm disks with scissors.

Characterization. SEM was performed using TESCAN MIRA 3LMU (Tescan Orsay Holding, a.s., Czech Republic). For EDX mapping, the graphite coating was used. Additional SEM and EDX images were recorded using the Quanta 200 3D, FEI, Hillsboro, and ORUSA system. The Thermo Fisher Scientific XPS NEXSA spectrometer with a monochromated Al K Alpha X-ray source working at 1486.6 eV was used for XPS. The survey spectra were recorded with the pass energy of 200 eV and an energy resolution of 1 eV. For the high-resolution spectra, the pass energy was 50 eV and the energy resolution was equal to 0.1 eV. The spot area was 200 μm^2. The flood gun was used for the charge compensation.

Raman measurements were performed after each step of textile modification to track the changes in material composition. Spectra were recorded using an NT-MDT-Solar AFM/Raman setup. The 532 nm laser was used for sample characterization using a 20x objective with a 1 s exposure time, 60 times accumulation, and 40 μW of laser power. SERS measurements were made using the same equipment and laser wavelength.

The MST 4000A microprobe station (MS Tech Korea Co., Ltd., South Korea) was used to place the tips on the rGO/textile sample (10 by 10 mm) in a square configuration with a side of 400 μm. Electrical characterization was performed on the potentiostat-galvanostat P-45X (Electrochemical Instruments, Russia). Sheet resistance was calculated using the equation

$$R_{\text{sheet}} = \frac{2\pi}{\ln 2}\frac{V}{I}$$

where V [V] is the voltage drop between two probes in the top pair of electrodes, and I [A] is the current applied by a pair of electrodes at the bottom. This method was used for several measurements, including stability after washing, keeping the samples in PBS, and in artificial sweat.

The photothermal activity was investigated using two light sources: (1) the LED lamp (3 W, 150 lm) was used to illuminate the rGO/textile and the pristine textile separately for 6 min. The temperature was measured by the HT-02 thermal imaging camera (HTI, China) before and after illumination without turning off the light source. (2) The halogen lamp of the "Micromed 3 lum" microscope was used as a light source. The same thermal imaging camera was fixed at 20 cm from the samples. We separately put rGO/textile and pristine textiles on the lamp's diffuser. Each sample was illuminated for 20 s with thermal imaging right afterward.

A Gotech ai-7000 Universal testing machine was used to perform a strain−stress test. Pristine textile and rGO/textile samples were cut following the dimensions of 40 × 10 × 0.5 mm^3. The working length of the sample was fixed at 19 mm.

Antibacterial Activity. A Gram-negative bacterial strain—*E. coli* (B-11333)—and a Gram-positive bacterial strain—*St. aureus* (B-6646)—were used here for antibacterial activity testing. Cultivation of *E. coli* was carried out on a dense nutrient medium Luria−Bertani (LB) incubated at 37 °C for 24 h. Bacteria *St. aureus* was grown in a liquid nutrient medium of beef-extract broth. The cultivation was carried out in an orbital shaker at 37 °C and a rotation frequency of 100 rpm for 24 h. Finally, a suspension of each bacterial species with a concentration of 3 units according to the McFarland turbidity standard was prepared and used in further tests. One day before the antibacterial activity test, a 1% agar solid nutrient medium was prepared, poured into Petri dishes (D = 90 mm), and kept for 24 h in a thermostat at 28−30 °C to control sterility. The 300 μL of suspension of each bacterial culture was applied to the agar surface and evenly spread over the surface with a Drigalski spatula. Samples under investigation were placed on the dried nutrient medium using tweezers (the treated side was placed on the surface of the nutrient medium). Finally, Petri dishes with samples were placed in an incubator at 37 °C for 48 h. The antibacterial effect on the samples was determined in transmitted light, estimating the width of the

https://doi.org/10.1021/acsami.3c06968
ACS Appl. Mater. Interfaces XXXX, XXX, XXX−XXX

inhibition zone of bacterial growth from the edge of the sample. The results were expressed in mm and presented as mean ± SD.

Sensor Performance. The research was conducted with the permission of Ethical Committee 7858/1 from 17.06.2020. We made 30 × 10 mm rGO/textile composites for both voice recognition and pulse sensing. For voice recognition, we fixed a sample right over the laryngeal prominence with the composite layer on top. Potentiostat/galvanostat P-45X (Electrochemical Instruments, Russia) was used for signal recording. The constant current of 2 mA was applied, and voltage changes were recorded. The same sensor was used for pulse recording and fixed on the carotid artery. The muscle activity sensor represents a 200 × 15 mm rGO/textile strip deposited on kinesiology tape with a composite layer on the tape. The sensor was wrapped around the forearm closer to the elbow. Applying a constant current of either 10 μA or 20 μA, we recorded the voltage over time diagram with a P-45X potentiostat.

Washing. The rGO/textile sample was placed in 150 mL of tap water with 1 mL of liquid soap. Three rubber balls of 2.5 cm in diameter were added. Washing was carried out at 40 rpm for 20 min. The samples were then dried on a heating plate at 50 °C. Sheet resistance values were measured using the 4-probe method or multimeter before and after washing.

■ ASSOCIATED CONTENT

Supporting Information

The Supporting Information is available free of charge at https://pubs.acs.org/doi/10.1021/acsami.3c06968.

Additional experimental findings, including photos of the samples, and experimental results on the formation of LIG using different textiles as the precursors; XPS analysis of nylon, rGO/textiles, Ag/rGO/textiles, and sheet resistance changes after different sonication times and after 5 washing cycles; evaluation of textile performance after keeping in PBS and artificial sweat; results of the adhesion test and stress−strain test; signals registered using different gestures and pronounciation of different sounds, thermal images under applying different voltage, and photothermal properties of rGO/textiles; SEM and EDX images of Ag/rGO/textiles (PDF)

■ AUTHOR INFORMATION

Corresponding Authors

Chong Cheng − *College of Polymer Science and Engineering, State Key Laboratory of Polymer Materials Engineering, Department of Ultrasound, West China Hospital, Sichuan University, Chengdu 610065, China;* orcid.org/0000-0002-6872-2240; Email: chong.cheng@scu.edu.cn

Raul D. Rodriguez − *Tomsk Polytechnic University, Tomsk 634034, Russia;* orcid.org/0000-0003-4016-1469; Email: raul@tpu.ru

Authors

Anna Lipovka − *Tomsk Polytechnic University, Tomsk 634034, Russia;* orcid.org/0000-0002-2012-1569

Maxim Fatkullin − *Tomsk Polytechnic University, Tomsk 634034, Russia*

Sergey Shchadenko − *Tomsk Polytechnic University, Tomsk 634034, Russia;* orcid.org/0000-0002-3391-2925

Ilia Petrov − *Tomsk Polytechnic University, Tomsk 634034, Russia*

Anna Chernova − *Tomsk Polytechnic University, Tomsk 634034, Russia*

Evgenii Plotnikov − *Tomsk Polytechnic University, Tomsk 634034, Russia*

Vitaliy Menzelintsev − *Tomsk Polytechnic University, Tomsk 634034, Russia*

Shuang Li − *College of Polymer Science and Engineering, State Key Laboratory of Polymer Materials Engineering, Department of Ultrasound, West China Hospital, Sichuan University, Chengdu 610065, China;* orcid.org/0000-0001-7414-630X

Li Qiu − *College of Polymer Science and Engineering, State Key Laboratory of Polymer Materials Engineering, Department of Ultrasound, West China Hospital, Sichuan University, Chengdu 610065, China;* orcid.org/0000-0003-2685-9799

Evgeniya Sheremet − *Tomsk Polytechnic University, Tomsk 634034, Russia*

Complete contact information is available at: https://pubs.acs.org/10.1021/acsami.3c06968

Author Contributions

A. Lipovka: conceptualization, investigation, validation, formal analysis, visualization, supervision, writing—original draft, and writing—review and editing. **M. Fatkullin:** conceptualization, investigation, validation, formal analysis, visualization, supervision, and writing—review and editing. **S. Shchadenko:** investigation, validation, formal analysis, writing—original draft, and writing—review and editing. **I. Petrov:** investigation, validation, formal analysis, visualization, writing—original draft, and writing—review and editing. **A. Chernova:** investigation, validation, formal analysis, writing—original draft, and writing—review and editing. **E. Plotnikov:** investigation, validation, formal analysis, writing—original draft, and writing—review and editing. **V. Menzelintsev:** investigation, validation, formal analysis, writing—original draft, and writing—review and editing. **S. Li:** investigation, validation, formal analysis, writing—original draft, and writing—review and editing. **L. Qiu:** investigation, validation, formal analysis, writing—original draft, and writing—review and editing. **C. Cheng:** investigation, validation, formal analysis, writing—original draft, and writing—review and editing. **R. D. Rodriguez:** conceptualization, investigation, validation, formal analysis, visualization, supervision, and writing—review and editing. **E. Sheremet:** writing—review and editing and funding acquisition.

Notes

The authors declare no competing financial interest.

■ ACKNOWLEDGMENTS

This research was supported by the project Priority 2030-NIP/IZ-007-0000-2022. Work was conducted with the application of equipment of the Tomsk Regional Core Shared Research Facilities Center of National Research Tomsk State University. The authors thank the central laboratories of TPU (the Analytical Center) for the XPS measurements and Alina Gorbunova for operating the equipment. The authors thank Varnika Prakash, Aura Garcia, Elizaveta Konstantinova, and Ilia Bril for their help at different stages of this research. The authors also thank Elizaveta Dogadina for the help with corrections to the Table of contents.

■ REFERENCES

(1) Luo, H.; Gao, B. Development of Smart Wearable Sensors for Life Healthcare. *Engineered Regeneration* **2021**, *2*, 163−170.

(2) Choudhry, N. A.; Arnold, L.; Rasheed, A.; Khan, I. A.; Wang, L. Textronics—A Review of Textile-based Wearable Electronics. *Adv. Eng. Mater.* **2021**, *23*, 2100469.
(3) Liu, H.; Zhong, X.; He, X.; Li, Y.; Zhou, N.; Ma, Z.; Zhu, D.; Ji, H. Stretchable Conductive Fabric Enabled By Surface Functionalization of Commercial Knitted Cloth. *ACS Appl. Mater. Interfaces* **2021**, *13*, 55656−55665.
(4) Lu, X.; Shang, W.; Chen, G.; Wang, H.; Tan, P.; Deng, X.; Song, H.; Xu, Z.; Huang, J.; Zhou, X. Environmentally Stable, Highly Conductive, and Mechanically Robust Metallized Textiles. *ACS Appl. Electron. Mater.* **2021**, *3*, 1477−1488.
(5) Wang, D.; Li, D.; Zhao, M.; Xu, Y.; Wei, Q. Multifunctional Wearable Smart Device Based on Conductive Reduced Graphene Oxide/polyester Fabric. *Appl. Surf. Sci.* **2018**, *454*, 218−226.
(6) Paul, G.; Torah, R.; Beeby, S.; Tudor, J. Novel Active Electrodes for ECG Monitoring on Woven Textiles Fabricated by Screen and Stencil Printing. *Sens. Actuators, A* **2015**, *221*, 60−66.
(7) Zhou, Z.; Li, Y.; Cheng, J.; Chen, S.; Hu, R.; Yan, X.; Liao, X.; Xu, C.; Yu, J.; Li, L. Supersensitive All-Fabric Pressure Sensors Using Printed Textile Electrode Arrays for Human Motion Monitoring and Human−machine Interaction. *J. Mater. Chem. C Mater. Opt. Electron. Devices* **2018**, *6*, 13120−13127.
(8) Li, Q.; Wu, T.; Zhao, W.; Ji, J.; Wang, G. Laser-Induced Corrugated Graphene Films for Integrated Multimodal Sensors. *ACS Appl. Mater. Interfaces* **2021**, *13*, 37433−37444.
(9) Lipovka, A.; Petrov, I.; Fatkullin, M.; Murastov, G.; Ivanov, A.; Villa, N. E.; Shchadenko, S.; Averkiev, A.; Chernova, A.; Gubarev, F.; Saqib, M.; Sheng, W.; Chen, J.-J.; Kanoun, O.; Amin, I.; Rodriguez, R. D.; Sheremet, E. Photoinduced Flexible Graphene/polymer Nanocomposites: Design, Formation Mechanism, and Properties Engineering. *Carbon N. Y.* **2022**, *194*, 154−161.
(10) Rodriguez, R. D.; Shchadenko, S.; Murastov, G.; Lipovka, A.; Fatkullin, M.; Petrov, I.; Tran, T.; Khalelov, A.; Saqib, M.; Villa, N. E.; Bogoslovskiy, V.; Wang, Y.; Hu, C.; Zinovyev, A.; Sheng, W.; Chen, J.; Amin, I.; Sheremet, E. Ultra-Robust Flexible Electronics by Laser-Driven Polymer-Nanomaterials Integration. *Adv. Funct. Mater.* **2021**, *31*, 2008818.
(11) Tania, I. S.; Ali, M.; Arafat, M. T. Processing Techniques of Antimicrobial Textiles. *Antimicrobial Textiles from Natural Resources*; Elsevier, 2021; pp 189−215.
(12) Usher, B. Human Sweat as a Culture Medium for Bacteria. *Arch. Derm. Syphilol.* **1928**, *18*, 276.
(13) Pullangott, G.; Kannan, U.; Gayathri, S.; Kiran, D. V.; Maliyekkal, S. M. A Comprehensive Review on Antimicrobial Face Masks: An Emerging Weapon in Fighting Pandemics. *RSC Adv.* **2021**, *11*, 6544−6576.
(14) Dastjerdi, R.; Montazer, M. A Review on the Application of Inorganic Nano-Structured Materials in the Modification of Textiles: Focus on Anti-Microbial Properties. *Colloids Surf. B Biointerfaces* **2010**, *79*, 5−18.
(15) Abid, J. P.; Wark, A. W.; Brevet, P. F.; Girault, H. H. Preparation of Silver Nanoparticles in Solution from a Silver Salt by Laser Irradiation. *Chem. Commun.* **2002**, *7*, 792−793.
(16) Seidi, F.; Deng, C.; Zhong, Y.; Liu, Y.; Huang, Y.; Li, C.; Xiao, H. Functionalized Masks: Powerful Materials against COVID-19 and Future Pandemics. *Small* **2021**, *17*, No. e2102453.
(17) Zhang, Y.; Guo, L.; Wei, S.; He, Y.; Xia, H.; Chen, Q.; Sun, H.-B.; Xiao, F.-S. Direct Imprinting of Microcircuits on Graphene Oxides Film by Femtosecond Laser Reduction. *Nano Today* **2010**, *5*, 15−20.
(18) Thapliyal, V.; Alabdulkarim, M. E.; Whelan, D. R.; Mainali, B.; Maxwell, J. L. A Concise Review of the Raman Spectra of Carbon Allotropes. *Diam. Relat. Mater.* **2022**, *127*, 109180.
(19) Balachandran, U.; Eror, N. G. Raman Spectra of Titanium Dioxide. *J. Solid State Chem.* **1982**, *42*, 276−282.
(20) Menchaca, C.; Alvarez-Castillo, A.; Martinez-Barrera, G.; Lopez-Valdivia, H.; Carrasco, H.; Castano, V. M. Mechanisms for the Modification of Nylon 6,12 by Gamma Irradiation. *Int. J. Mater. Prod. Technol.* **2003**, *19*, 521.
(21) Ma, B.; Rodriguez, R. D.; Ruban, A.; Pavlov, S.; Sheremet, E. The Correlation between Electrical Conductivity and Second-Order Raman Modes of Laser-Reduced Graphene Oxide. *Phys. Chem. Chem. Phys.* **2019**, *21*, 10125−10134.
(22) Nguyen, V. T.; Le, H. D.; Nguyen, V. C.; Tam Ngo, T. T.; Le, D. Q.; Nguyen, X. N.; Phan, N. M. Synthesis of Multi-Layer Graphene Films on Copper Tape by Atmospheric Pressure Chemical Vapor Deposition Method. *Adv. Nat. Sci. Nanosci. Nanotechnol.* **2013**, *4*, 035012.
(23) Huh, S. H. Thermal reduction of graphene oxide. In *Physics and Applications of Graphene: Experiments*; Mikhailov, S., Ed.; InTech, 2011; pp 73−90.
(24) Cai, G.; Xu, Z.; Yang, M.; Tang, B.; Wang, X. Functionalization of Cotton Fabrics through Thermal Reduction of Graphene Oxide. *Appl. Surf. Sci.* **2017**, *393*, 441−448.
(25) Pan, Q.; Shim, E.; Pourdeyhimi, B.; Gao, W. Nylon-Graphene Composite Nonwovens as Monolithic Conductive or Capacitive Fabrics. *ACS Appl. Mater. Interfaces* **2017**, *9*, 8308−8316.
(26) Moreira, V. R.; Lebron, Y. A. R.; da Silva, M. M.; de Souza Santos, L. V.; Jacob, R. S.; de Vasconcelos, C. K. B.; Viana, M. M. Graphene Oxide in the Remediation of Norfloxacin from Aqueous Matrix: Simultaneous Adsorption and Degradation Process. *Environ. Sci. Pollut. Res. Int.* **2020**, *27*, 34513−34528.
(27) Zhong, Y.; Tan, X.; Shi, T.; Huang, Y.; Cheng, S.; Chen, C.; Liao, G.; Tang, Z. Tunable Wrinkled Graphene Foams for Highly Reliable Piezoresistive Sensor. *Sens. Actuators, A* **2018**, *281*, 141−149.
(28) Yang, H.; Xue, T.; Li, F.; Liu, W.; Song, Y. Graphene: Diversified Flexible 2D Material for Wearable Vital Signs Monitoring. *Adv. Mater. Technol.* **2018**, *4*, 1800574.
(29) Avram, R.; Tison, G. H.; Aschbacher, K.; Kuhar, P.; Vittinghoff, E.; Butzner, M.; Runge, R.; Wu, N.; Pletcher, M. J.; Marcus, G. M.; Olgin, J. Real-World Heart Rate Norms in the Health eHeart Study. *NPJ Digit Med* **2019**, *2*, 58.
(30) Habash, R. W. Y.; Bansal, R.; Krewski, D.; Alhafid, H. T. Thermal Therapy, Part 1: An Introduction to Thermal Therapy. *Crit. Rev. Biomed. Eng.* **2006**, *34*, 459−489.
(31) Henwood, A. F. Coronavirus Disinfection in Histopathology. *J. Histotechnol.* **2020**, *43*, 102−104.
(32) Babaahmadi, V.; Montazer, M.; Gao, W. Low Temperature Welding of Graphene on PET with Silver Nanoparticles Producing Higher Durable Electro-Conductive Fabric. *Carbon* **2017**, *118*, 443−451.
(33) Gurunathan, S.; Woong Han, J.; Abdal Daye, A.; Eppakayala, V.; Kim, J.-H. Oxidative Stress-Mediated Antibacterial Activity of Graphene Oxide and Reduced Graphene Oxide in Pseudomonas Aeruginosa. *Int. J. Nanomed.* **2012**, *7*, 5901−5914.
(34) Liu, S.; Zeng, T. H.; Hofmann, M.; Burcombe, E.; Wei, J.; Jiang, R.; Kong, J.; Chen, Y. Antibacterial Activity of Graphite, Graphite Oxide, Graphene Oxide, and Reduced Graphene Oxide: Membrane and Oxidative Stress. *ACS Nano* **2011**, *5*, 6971−6980.
(35) Barbolina, I.; Woods, C. R.; Lozano, N.; Kostarelos, K.; Novoselov, K. S.; Roberts, I. S. Purity of Graphene Oxide Determines Its Antibacterial Activity. *2D Materials* **2016**, *3*, 025025.
(36) Endo-Kimura, M.; Kowalska, E. Plasmonic Photocatalysts for Microbiological Applications. *Catalysts* **2020**, *10*, 824.
(37) Bruna, T.; Maldonado-Bravo, F.; Jara, P.; Caro, N. Silver Nanoparticles and Their Antibacterial Applications. *Int. J. Mol. Sci.* **2021**, *22*, 7202.
(38) Koh, E. H.; Lee, W.-C.; Choi, Y.-J.; Moon, J.-I.; Jang, J.; Park, S.-G.; Choo, J.; Kim, D.-H.; Jung, H. S. A Wearable Surface-Enhanced Raman Scattering Sensor for Label-Free Molecular Detection. *ACS Appl. Mater. Interfaces* **2021**, *13*, 3024−3032.
(39) Xiao, G.-N.; Man, S.-Q. Surface-Enhanced Raman Scattering of Methylene Blue Adsorbed on Cap-Shaped Silver Nanoparticles. *Chem. Phys. Lett.* **2007**, *447*, 305−309.
(40) Sooraj, K. P.; Ranjan, M.; Rao, R.; Mukherjee, S. SERS Based Detection of Glucose with Lower Concentration than Blood Glucose Level Using Plasmonic Nanoparticle Arrays. *Appl. Surf. Sci.* **2018**, *447*, 576−581.

https://doi.org/10.1021/acsami.3c06968
ACS Appl. Mater. Interfaces XXXX, XXX, XXX−XXX

(41) Zafar, H.; Channa, A.; Jeoti, V.; Stojanović, G. M. Comprehensive Review on Wearable Sweat-Glucose Sensors for Continuous Glucose Monitoring. *Sensors* **2022**, *22*, 638.

https://doi.org/10.1021/acsami.3c06968
ACS Appl. Mater. Interfaces XXXX, XXX, XXX−XXX